CHARACTERIZATION OF WELD HEAT INPUT EFFECTS ON MECHANICAL PROPERTIES OF Cr-Mo STEEL BAR USING TIG WELDING PROCESS

Reuben Adebare ADEWUYI[1,*], Jacob Olayiwola AWEDA[2]

[1]Department of Mechanical Engineering, The Federal Polytechnic, Ado-Ekiti, Nigeria.
[2]Department of Mechanical Engineering, University of Ilorin, Ilorin, Nigeria.

Abstract

Welding as an energy-consuming process is inevitable as-welded joint can be subject to various loads without failure. Therefore, this paper presents the welding thermal cycle of Cr-Mo steel bar (ASTM A304) of dimensions 100 by 50 and various thicknesses of 5, 10- and 15-mm. Pure tungsten with 2% thoriated TIG electrodes sizes 1.6 mm X 175 mm, 2.4 mm X 175 mm, and 3.2 mm X 175 were used without filler materials for the welding process. A double V-groove weld joint, with a moving heat source, was employed to determine the temperature fields and transformation in the single-pass butt-welded joint. A calibration process was attached at each point of interest using a datalogger type K-type thermocouple 3-channel–LU-MTM-380SD during the welding process on the Cr-Mo steel bar. The results showed that the welding temperature became higher at the welding centreline and decreased towards the edges of the bar. An indication that a weld thermal cycle is a veritable tool, a function of heat input to access likely consequence of the welding process at both welded and parent metal portions of steel bar. Design of Experiment using Taguchi L9 orthogonal array matrix L9(3^4), Factors:4 and Runs:18 in Minitab 17 Taguchi Design Method that suited the experimental method used. Taguchi's L9 orthogonal array to restrict the number of experimental runs was used for the design of the experiment (DOE). Mechanical and Microstructure tests were carried out on the samples to investigate the effect of weld heat input. The hardness test result showed that samples C15 and D15 have the highest hardness values 165.0HV and 164.0HV respectively at Base metal (BM) 20mm away from weld centreline and it was also observed that samples C15 and D15 have the highest impact values 48.53J and 48.7J respectively. The microstructure of the C15 at the weld zone WZ, which consists majorly of pearlite and less ferrite, BM shows the appearance of alpha ferrite and pearlite and heat-affected zone HAZ consists majorly of pearlite and a very small proportion of ferrite resulted in increased hardness and impact values at the HAZ.

Keywords*: weld joints, thermal cycle, welding parameters, heat input.*

Introduction

Welding as materials joining process is inevitable in achieving industrial development set goals. The effect of the material thickness, weld heat source (current), electrode diameter, and weld pass on temperature distribution were investigated.

The Cr-Mo steel bar (ASTM A304) of dimensions 100x50x5mm, 100x50x10mm, and 100x50x15mm was used as a workpiece material for this study. Pure tungsten with 2% Thoriated TIG Electrodes sizes Ø1.6x175mm, Ø2.4x175mm, and Ø3.2x175mm are used without filler materials for the weld joining process. Welding is the main focus in metal fabrication which is a process of joining different metals or materials [1].

*Corresponding author: reuben1178@yahoo.com

In welding, different welding parameters like welding current, arc voltage, welding speed, electrode feed speed, electrode diameter, electrode extension, and joint geometry influence the weld quality and weld deposition rates during the welding operation. TIG Welding process depends mostly on welding parameters set to generate arc energy that is transferred as weld heat input to the weldment [2,3]. The total weld heat input is transferred to the weldment per unit time, per unit length of the weld. The non-consumable Tungsten electrode is continuously fed into the melt to maintain a constant arc length, in which the heat transfer from the end of the non-consumable electrode to the workpiece has a considerable effect on the weldment characteristics, so they are the primary parameter in the welding process [4,5]. The mechanical properties and microstructures of welded Cr-Mo steels structure could be altered during TIG welding operations [6,7].

When welding current and voltage are kept constant but welding speed is varied, changes in weld penetration are due to different heat input rates per arc length. Effects of welding parameters such as heat-input, filler metal composition, and the number of weld passes, on the mechanical properties and influence on the microstructure, were studied to minimize cold cracking and provide adequate weld zone toughness for resistance to fatigue cracking [8].

Failure of welded Cr-Mo steel bar at weld joints while in service is a common phenomenon that has led to several structural failures as a result of differences in material properties especially yield stress between base metal, weldment and heat affected zone is considered in order to minimise structural failure rate [9]. In some industries, TIG welding joints could be a difficult task with the problem of cracks and altered mechanical properties of weldment compared to the parent material due to differential heating and cooling causing non-uniform volumetric changes. These non-uniform volumetric changes affect the heating, soaking, and cooling cycle of the workpiece which affects the metallurgical and mechanical properties, which this paper tries to solve. In this research work, "Characterization of weld heat input effects on mechanical and microstructural properties of Cr-Mo steel bar using TIG welding process" is considered.

Weld thermal cycle at the three points of interest

Figure 1 showed variation in temperature difference at each point of interest (in and around the weldment) as a function of welding parameters. As the heat source approaches the points of interest; T1, T2, and T3, a non-uniform volumetric change in temperature explained, the rate of heating (PQ), peak temperature (Q) and time required for attaining the peak temperature, cooling rate (QR) as shown in Figure 1 [9].

Methodology

Table 1 showed the Chromium-Molybdenum steel bar contains carbon, magnesium, silicon, chromium, molybdenum, and iron at 0.04%, 0.15%, 0.08%, 17.62%, 0.55% and 72.98% compositions as the main elements plus traces of other elements. Similar observations were reported by [10,11] though occurring at a slightly higher value.

Table 1. Chemical Composition (wt %) of as-received Cr-Mo steel bar (ASTM A304)

Element	C	Mn	Si	P	S	Cr	Ni	Mo	N	Fe
Concentration (wt. %)	0.04	0.15	0.08	0.02	0.02	17.62	8.47	0.55	0.07	72.98
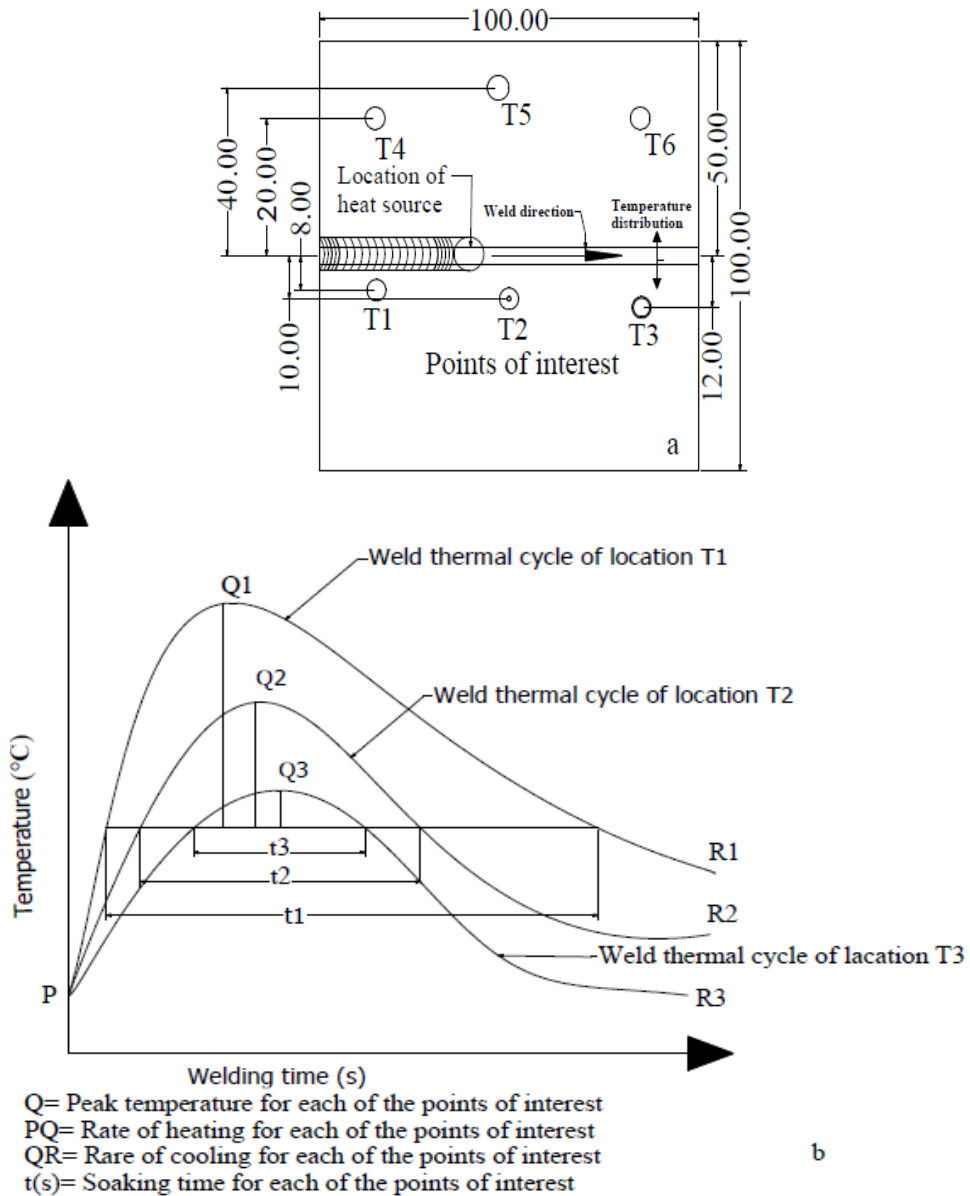
Fig. 1. a) Typical points of interest and b) weld thermal cycle

Design of Experiment using Taguchi Design Method

Experimental Design for 50mm by 100mm in pairs from 5mm,10mm, and 15mm Cr-Mo steel bar for the welding operation is presented in Tables 2. *Minitab 17* was used to design of Experiment using Taguchi L9 orthogonal array matrix L9(3^4), Factors: 4 and Runs: 18 are shown in Table 3.

Welding constant parameters

Electrode type: 98% tungsten, 2% thoriated; Shielded gas type: pure argon; Flow rate: 10-12 l/min; Voltage: 24 V [9].

Table 2. TIG Welding process parameter and parameter levels [11]

Parameters	Level-1	Level-2	Level-3
Material Thickness (mm)	5	10	15
Welding Current(A)	90	110	150
Welding Pass	1	1	1
Electrode diameter (Ø mm)	1.6	2.4	3.2

Table 3. Design of Experiment using Taguchi L9 orthogonal array

Exp no	Material Thickness (mm)	Welding Current (A)	Number of weld pass	Electrode Diameter (Ømm)	Sample ID	Remarks
1	5	90	1	1.6	A5	Carried out
2	5	90	1	1.6	B5	Carried out
3	5	110	2	2.4	C5	
4	5	110	2	2.4	D5	
5	5	150	3	3.2	E5	
6	5	150	3	3.2	F5	
7	10	90	2	3.2	A10	
8	10	90	2	3.2	B10	
9	10	110	3	1.6	C10	
10	10	110	3	1.6	D10	
11	10	150	1	2.4	E10	Carried out
12	10	150	1	2.4	F10	Carried out
13	15	90	3	2.4	A15	
14	15	90	3	2.4	B15	
15	15	110	1	3.2	C15	Carried out
16	15	110	1	3.2	D15	Carried out
17	15	150	2	1.6	E15	
18	15	150	2	1.6	F15	

The Cr-Mo steel of 5, 10 and 15mm thicknesses were used for this research work which was cut in pairs to size 100x50mm from different thicknesses,18 samples of the Cr-Mo steel bar type under consideration. Before welding operation, on each pair, a hole of 5.0mm was drilled and tapped close to the weld centreline of the samples, where a K type thermocouple of 2000^0C capacity was connected to each of the points of interest to measure the weld thermal cycle between the base metal and welded bead. The arc welding temperature (1350…1400°C) was recorded using Digital Infrared Thermometer Ametek LAND Cyclops 100L S/N 240671 91. The weld thermal cycle at the selected points of interest was recorded at 5-second intervals. The joint configuration for the welded design was the Double V-butt weld joint and the selection of joint design for the required static strength is a primary criterion.

Figure 2 showed a typical experimental procedure during the welding operation. To investigate the temperature distribution in the welded steel bars, three points were selected for the measurement (Fig. 3). For each assembly, three thermocouple wires were attached to the specimen at points 8, 10, and 12 mm away from the weld centreline, respectively. Thermocouples (type K) were used to record the weld thermal cycle at each point of interest.

Fig. 2. Typical experimental procedure: 1-welding machine; 2-TIG torch;
3-Datalogger Datalogger with type K thermocouples –3 channel; 4-track

Fig. 3. The specimen showed: a) three k-type thermocouples planted at
different points of interest away from b) the weld centreline for faces

Results and discussion

Characterization of Cr-Mo steel bar (ASTM A304)
Chemical Compositional Analysis of Cr-Mo steel bar (ASTM A304)

Chemical Compositional Analysis of the as-received Cr-Mo steel bar was carried using scanning electron microscopy (SEM) and is presented in Table 4. The Chromium-Molybdenum steel bar contains carbon, magnesium, silicon, chromium, molybdenum, and iron at 0.04%, 0.15%, 0.08%, 17.62%, 0.55% and 72.98% compositions as the main elements plus traces of other elements. (see Table 4). Similar observations were reported by [10, 11] though occurring at a slightly higher value.

Table 4. Chemical Composition (wt %) of as-received Cr-Mo steel bar (ASTM A304)

Element	C	Mn	Si	P	S	Cr	Ni	Mo	N	Fe
Concentration (wt. %)	0.04	0.15	0.08	0.02	0.02	17.62	8.47	0.55	0.07	72.98

Elemental Compositional Analysis of Cr-Mo steel bar (ASTM A304)

Fig. 4 a-c showed the results of elemental compositions of Cr-Mo steel bar (ASTM A304) using an X-Ray Fluorescence (XRF) spectrometer. XRF is an elemental analytical technique and therefore quantify the total concentration of each element in a sample.
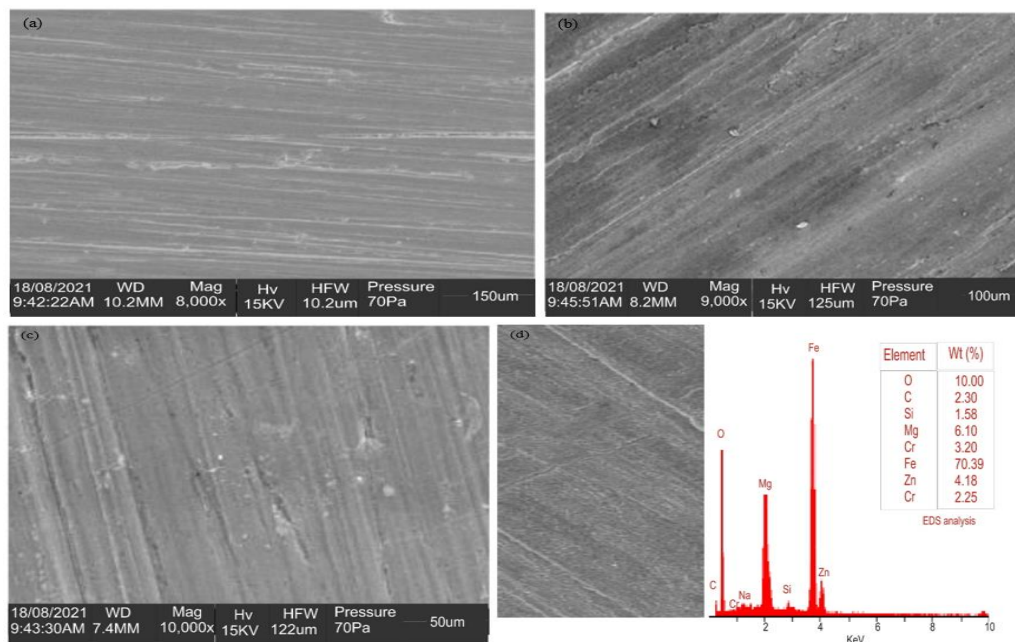
Fig. 4. XRF analysis of Cr-Mo steel bar (ASTM A304): a) Mag 8.000x 150μm; b) Mag 9.000x 100μm,; c) Mag 10.000x 50μm; d) total concentration of each element in the sample

Compound Compositional Analysis of Cr-Mo steel bar (ASTM A304)

Fig. 3 illustrates the XRD analysis of phase compositions of the Cr-Mo steel bar (ASTM A304). The figure depicts a shift of position in peaks. The diffraction peak values presented in Figure 5 were obtained at diffraction angles 2θ of 18.27, 21.34, 35.17and 65.45° corresponding to inter-planar distances 2.36, 2.76, 4.54 and 8.45 Å with the relative intensity of x-ray scattering 1000, 460, 2000, and 315 a-u respectively (Tammasophon *et al.*, 2011).

Temperature measurement at the three points of interest.

Datalogger with type K thermocouples –3 channel–LU-MTM-380SD was used to record the welding temperature field of weld thermal cycle at the three-point of interest and the recorded data was analysed graphical based on welding parameters set. The Arc welding temperature (1350…1450°C) was measured using Digital Infrared Thermometer Ametek Land Cyclops 100L S/N 240671 91.

The weld thermal cycles at the three-point of interest in the specimens A5, E10, and C15 during the welding process were presented in Figs. 6-8 and Tables 5-7 for the first weld pass on the two faces at different points. The peak temperature at point of interest T1: 429.8°C (860s), 432.9 °C (915s) and 431.5°C (920s); T2: 380.6°C (915s), 425.4°C (960s) and 418.7°C (970s); T3 :293.9°C (960s), 312.5°C (1005s) and 300.9°C (1015s) for specimens A5, E10 and C15 respectively. The heat input reaches the edges of the steel bar when the temperature continuously reduces to 58.6°C, 59.1°C, and 59.3°C for each of the specimens A5, E10, and C15 respectively, due to the effect of air cooling. This is because weld geometry parameters such as weld current and electrode diameter influenced the weld heat input distribution rate in steel bar for different weld thermal cycles [12, 13]

Sample	: Stainless	File	: Sg2~1.ASC	Date : August 19 8:20:28	Operator :
Comment	: Qualitative	Memo			
Method	: 2nd differential	Typica width : 0.065 deg.	Min. Height		2000:00 c p s
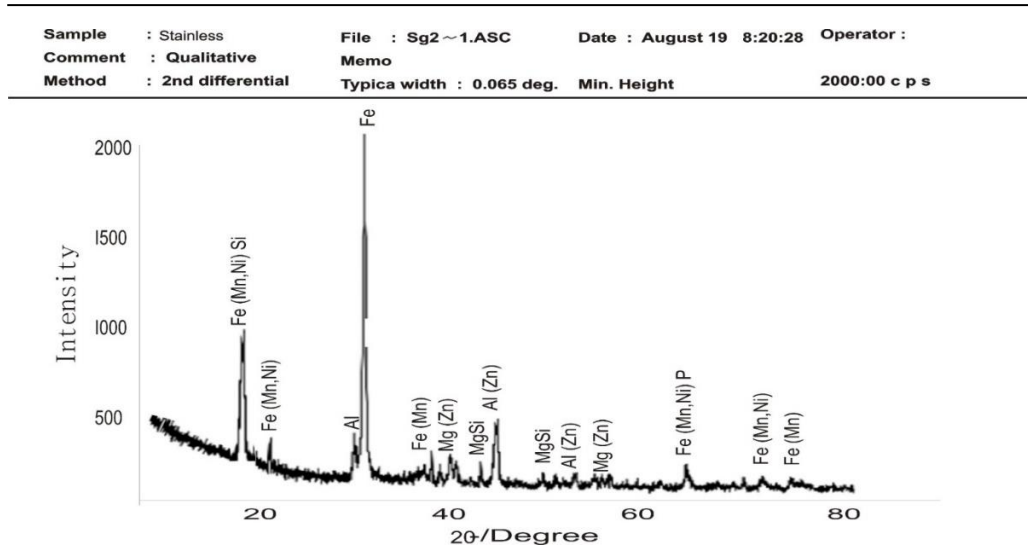
Fig. 5. XRD analysis of Cr-Mo steel bar (ASTM A304)

Figures 6-8 show the temperature time-histories of the experimental measurements on specimens A5, E10, and C15. There are two peak temperature values for each of the samples points of interest because of the double-v-butt weld type carried out on the specimens. In the measured points located 8mm, 10mm, and 12mm away from the weld centerline on the specimens, the temperature drops from 1450°C (Arc welding temperature of Cr-Mo steel bar) to less than 435 °C at each of the points.

In general, Figures 6-8 weld thermal cycle showed that, an increase in distance of the point of interest away from the weld centreline [9].

Table 5. Temperature fields in Cr-Mo steel bar (100x100x5mm) A5 during
TIG welding operation on the Double V-butt weld joint.

Machine setting/ weld parameters applied		
Material Thickness (mm)	5	SPECIMEN ID
Welding Current(A)	90	
Number of weld passes	1	A5
Electrode diameter (Ø mm)	1.6	

Table 6. Temperature fields in Cr-Mo steel bar (100x100x10mm) E10
during TIG welding operation on the Double V-butt weld joint

Machine setting/ weld parameters applied		
Material Thickness (mm)	10	Sample ID
Welding Current(A)	150	
Number of weld passes	1	E10
Electrode diameter (Ø mm)	2.4	

Table 7. Temperature fields in Cr-Mo steel bar (100x100x15mm) C15
during the TIG welding operation Double V-butt weld joint.

Machine setting/ weld parameters applied		
Material Thickness (mm)	15	Sample ID
Welding Current(A)	110	
Number of weld passes	1	C15
Electrode diameter (Ø mm)	3.2	
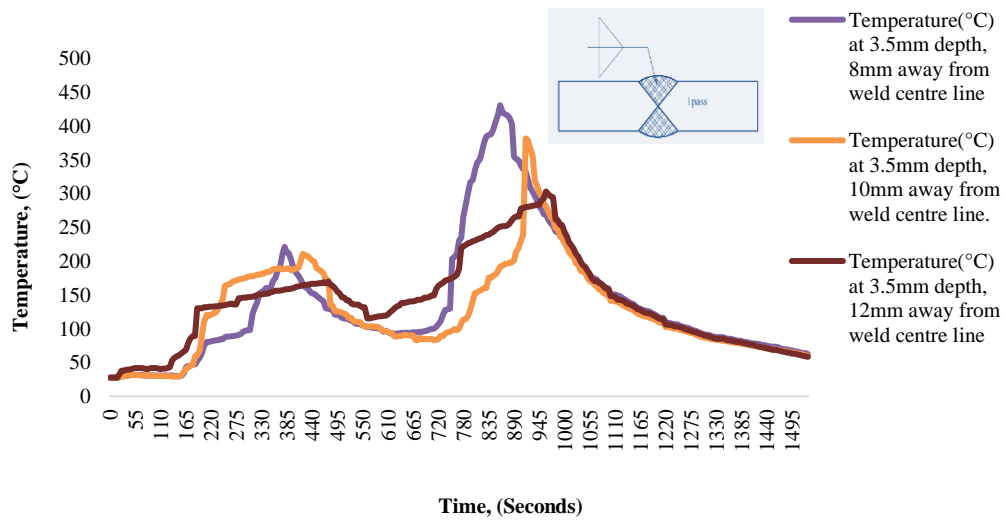
Fig. 6. Weld thermal cycle in Cr-Mo steel bar (100x100x5mm) specimen A5, at 8mm, 10mm & 12mm away from weld centreline
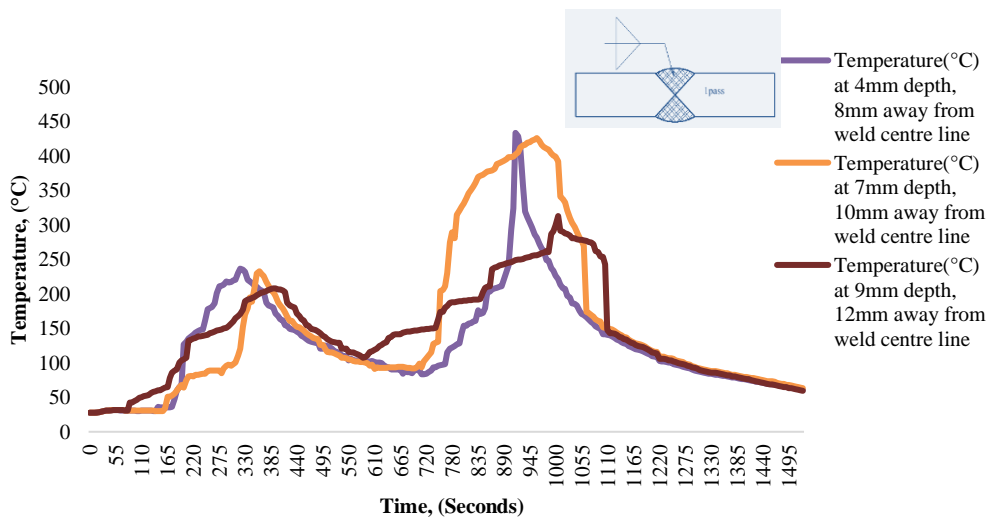
Fig. 7. Weld thermal cycle in Cr-Mo steel bar (100x100x10mm) specimen E10, at 8mm,10mm & 12mm away from weld centreline
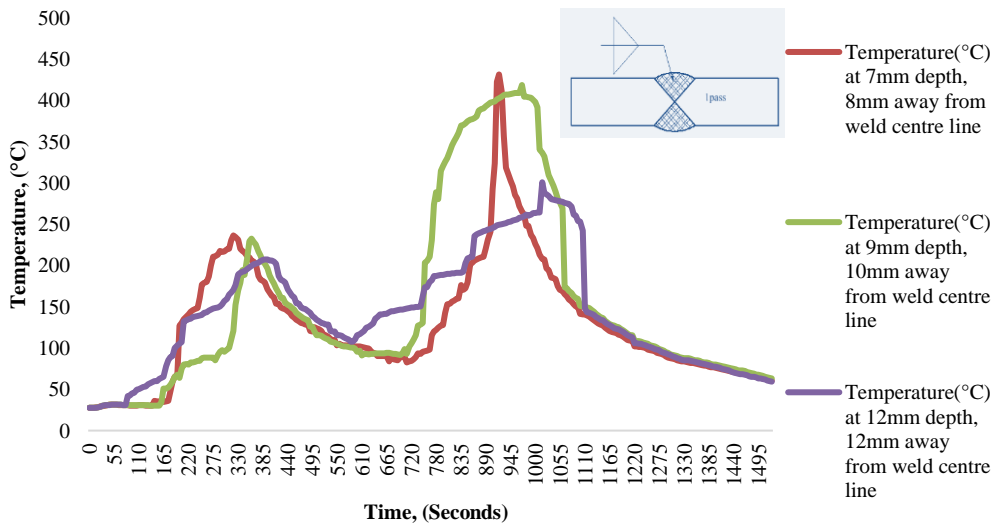
Fig. 8. Weld thermal cycle in Cr-Mo steel bar (100x100x15mm) specimen C15, at 8mm, 10mm & away from weld centreline

Hardness test on different thicknesses of Stainless-steel plate specimens.

The hardness properties of the specimens were determined using Brinell Hardness. The hardness properties of the seven samples with control were presented in Figure 9. Six tests were carried out on each sample. From the obtained results, it was observed that samples C15 and D15 have the highest hardness values (165.0HV and 164.0HV respectively) at Base metal BM 20mm away from weld centreline as shown in Figure 7. This shows the distribution of hardness values across the weldments of all specimens in which an increase in the magnitude of hardness values at the HAZ is visible. According to the results, C15 shows the highest increase when compared to other steels welded with different welding parameters.

Hardness vs Weldment samples

	WZ	FZ	HAZ	BM12mm	BM15mm	BM20mm
A5 (5mm, 90A,1 &1.6mm)	105	112	120	122	124	126
B5(5mm, 90A,1 &1.6mm)	107	114	117	122	122	123
E10(10mm, 150A,1 & 2.4mm)	115	123	140	148	150	151
F10(10mm, 150A,1 & 2.4mm)	110	119	125	128	129	130
C15 (15mm, 110A,1 & 3.2mm)	122	131	159	162	163	165
D15(15mm, 110A,1 & 3.2mm)	122	131	159	160	162	164
ASR (As Received)				95	89	124
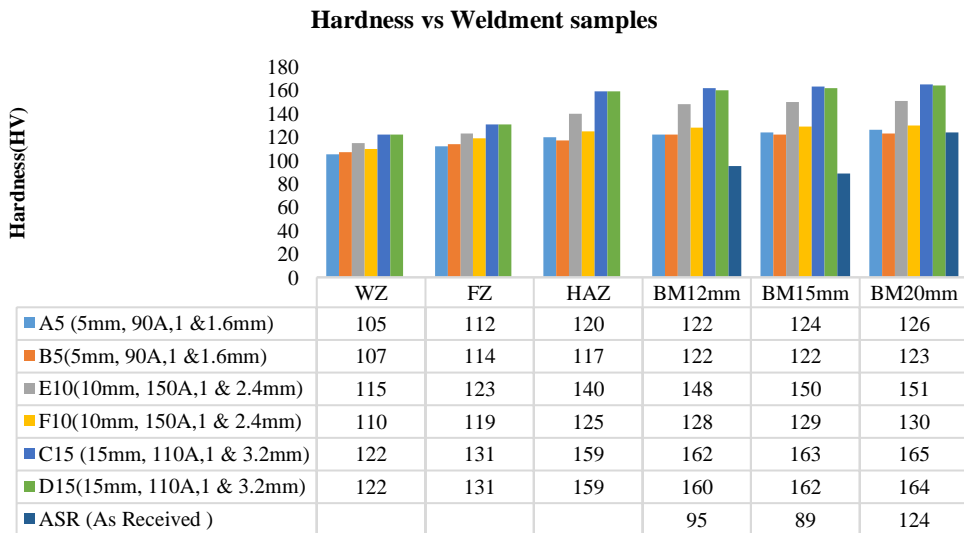
Fig. 9. Hardness distribution on the weldments with different welding parameters set

Impact test on different thicknesses of Stainless-steel plate specimens.
The properties of the specimens were determined using the Hounsfield Balanced Impact machine. The impact properties of the seven samples with control were presented in Figure 10. Four tests were carried out on each sample. From the obtained results, it was observed that samples C15 and D15 have the highest impact values (48.53J and 48.7J respectively) as shown in Figure 10.

Impact vs Weldment samples

	A5	B5	E10	F10	C 15	D 15	ASR
IMPACT (J)	38.31	43.38	41.07	45.33	48.53	48.7	34.24
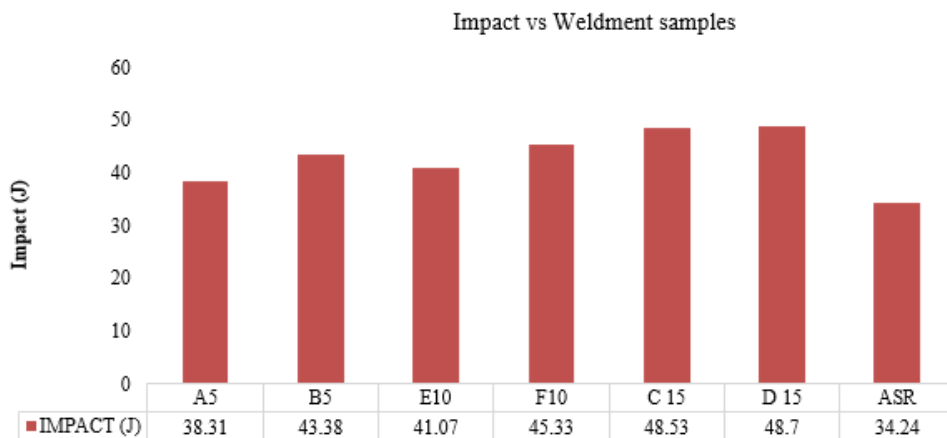
Fig. 10. Impact distribution on the weldments

Microstructure analysis
The microstructural analysis to reveal features of the welded specimens was carried out using SEM. To study the effect of weld heat input as a function of weld thermal cycle, that lead to the different microstructure of each weldment, three zones were considered: weld zone (WZ), heat-affected zone (HAZ), and base metal (BM) [9] after the first weld pass on each of the specimens. The microstructures were presented in Figures 11-13. The Figs. show the distribution of grains of ferrite and pearlite phases of the nature of failure from the resulting weldment and base metal. Therefore, the microstructure analysis was typically examined and presented in Figs. 11-13 using a scanning electron microscope (SEM/EDS). This clearly explained the effect of weld heat input on the mechanical properties of the weldments after welding.
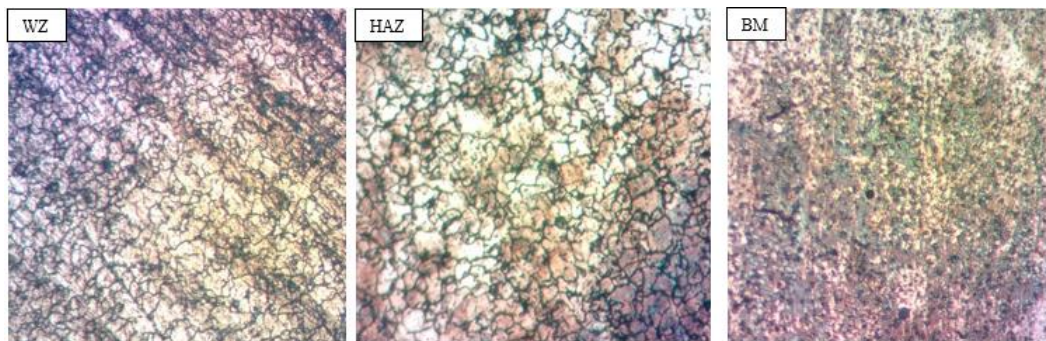
Fig. 11. The microstructural results for A5 at WZ, HAZ, and BM with magnification x640
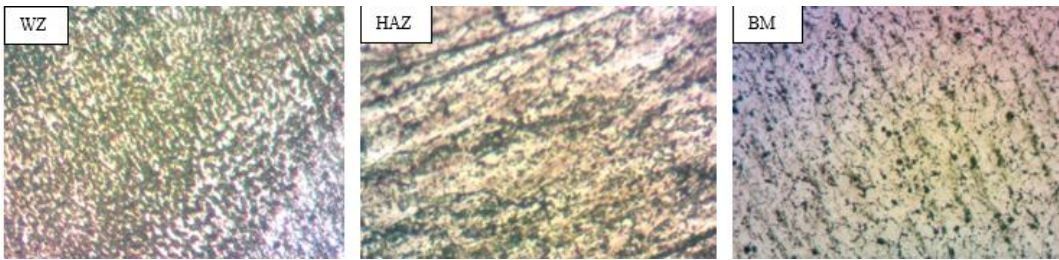
Fig. 12. The microstructural results for E10 at WZ, HAZ, and BM with magnification x640.
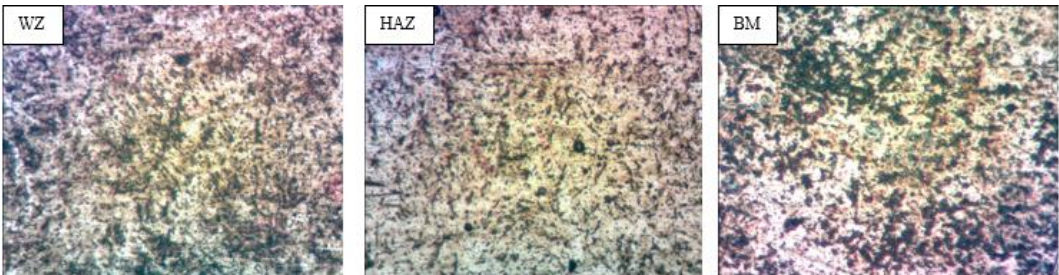
Fig. 13. The microstructural results for C15 at WZ, HAZ, and BM with magnification x640.

Figures 11-13 showed the distribution of steel phases, white grains represent Ferrite phase, and black grains are Pearlite phases, with Pearlite phases consisting of alternating layers of Ferrite and Cementite phases, present in the weld zone (WZ), heat affected zone (HAZ) and base metal (BM), thus has both soft and medium mechanical properties.

Figure 11 depicts the microstructure of the base metal, which consists of ferrite and pearlite with fine grains and closed grain boundaries. The microstructure of the weld zone also consists of pearlite and ferrite phases. The microstructure of the heat-affected zone consists of pearlite and ferrite with coarse grains. Thus, the weldment has low carbon content with soft mechanical properties.

Figure 12 presents the microstructure of the base metal, which consists of ferrite and pearlite with fine grains. The weld zone consists of pearlite majorly with a small proportion of ferrite and the heat-affected zone (HAZ) consists of ferrite and pearlite. Thus, the weldment has low carbon content with soft mechanical properties.

Figure 13 shows the microstructure of the base metal (BM) consists of pearlite phases (Black grains) with a small percentage of ferrite phases (White grains) indicating low carbon content with soft mechanical properties. The microstructure of the welded zone (WZ) consists of pearlite and ferrite, rough grains, and the grain boundaries are closed. The microstructure of the heat-affected zone (HAZ), consists of ferrite and pearlite. The grain phases are fine and the grain boundaries are closed. Thus, the weldment has low carbon content with soft mechanical properties.

Conclusions

From the results the following conclusions are drawn in respect of TIG-welded joints of ASTM A304 steel bar, based on experimental results and analysis:
- The highest experimentally obtained temperature is at the peak value of the curve closest to the weld centerline (T1=8 mm). The temperature effect reduces away from the weld centreline. The temperature at T1=8mm away from weld centerline is at its peak 429.8°C which is the highest and this is followed by the temperature at T2=10mm away from weld

centerline 380.6 $^{\circ}$C and the least which is at T3=12mm away from weld centerline 293.9 $^{\circ}$C. This showed that the temperature decreases when the distance between the measured point of interest and the weld centreline increases.

- The micro-hardness value of the weld zone is found to be remarkably higher as compared to those of the HAZ zone, base metal, and ASR. It is also found that all the welded joints exhibit a higher hardness value than that of the ASR. Also, it was observed that the hardness value increases as a point of interest move away from the weld centreline.
- Optimum hardness values of 165.0HV and 164.0HV respectively were observed for samples C15 and D15, highest hardness values at Base metal, BM 20mm away from weld centreline.
- The influence of welding parameters on impact property for samples C15 and D15 having the same weld parameters (110A, 15mm & Ø 3.2mm) is maximum with samples C15 and D15 having the highest impact values 48.53J and 48.7J respectively.
- Sample A5 and B5 having the same weld parameters (90A, 5mm & Ø 1.6mm) showed the highest tensile strength and this is due to the formation of equal percentage of Ferrite phase and pearlite phase that led to the highest strength and toughness.
- The microstructure of the C15 at the BM showed the appearance of ferrite phase and pearlite phase at weld zone (WZ), heat affected zone (HAZ), and base metal (BM), with closed grain boundaries.
- Figs. 6-8 showed the distribution of steel phases, white grains represent Ferrite phase, and black grains are Pearlite phases, with Pearlite phases consisting of alternating layers of Ferrite and Cementite phases, present in the weld zone (WZ), heat affected zone (HAZ) and base metal (BM), thus has both soft and medium mechanical properties indicating soft mechanical properties.

References

[1] Tailor, D. H., Srinivasan, K. N., Channiwala, S. A., Sohel, M., & Panwala, M., *Simulation of temperature field of TIG welding using FDM*. **American Society of Mechanical Engineers, Pressure Vessels, and Piping Division (Publication) PVP, 6(PART A),** 2008, pp. 515–521. https://doi.org/10.1115/PVP2009-77697

[2] Kaiser, M. S., *Effect of Heat Input on the Weld Metal Toughness of Chromium-Molybdenum Steel,* **International Scholarly and Scientific Research & Innovation**, 2013, 1 (7), pp. 33-35.

[3] Richard, G. B., & Nisbett, J. K., *Shigley's Mechanical Engineering Design.* (9th, Ed.) New York: McGraw-Hill, 2011.

[4] Chennaiah, B. M., Nanda, K. P., & Prahlada, R. K. *Effect of Heat Input and Heat Treatment on the Mechanical Properties of IS2062-IS103 Cr 1 steel Weldments,* **International Journal of Advances in Materials Science and Engineering**, 2015, 4, pp. 17-24.

[5] Xiang, J., Chen, F. F., Park, H., & Murphy, A. B., *Effects of Diffusion of Metal Vapour in an Argon TIG Welding Plasma,* Korea: CSIRO Manufacturing, 2018

[6] Kumslytis, V., Skindaras, R., & Valiulis, V., *The Structure and Properties of 5 % Cr-Mo. 5 % Mo Steel Welded Joints after Natural Ageing and Post-weld Heat Treatment*, **Materials Science Technology,** 2012, 18 (2), pp. 119-122.

[7] Boumerzoug, Z., Derfouf, C., & Baudin, T. *Effect of Welding on Microstructure and Mechanical Properties of an Industrial Low Carbon Steel*, **Engineering**, 2010, 2(7), pp. 502-506.

[8] Amraei, M., Ahola, A., Afkhami, S., Björk, T., Heidarpour, A., & Zhao, X. L. *Effects of heat input on the mechanical properties of butt-welded high and ultra-high-strength steels*, **Engineering Structures**, 2019, 198(June), 109460. doi: 10.1016/j.engstruct.2019.109460.

[9] Adewuyi, R. A., & Aweda, J. O. *Modeling and simulation of welding temperature fields in*

cr-mo steel bar, **European Journal of Materials Science and Engineering**, 2021, 6(1), pp. 3–18. doi: 10.36868/ejmse.2021.06.01.003

[10] Naik, A. B., *Effect of Process Parameters of Tungsten Inert Gas Welding on Welding of Duplex Stainless Steels,* **International Journal for Research in Applied Science and Engineering Technology**, 2018, *6*(1), pp. 2818–2827. doi: 10.22214/ijraset.2018.1388.

[11] Reddy, R., *Simulation of tig welding process simulation of tig welding*. Publisher: **LAP lambert academic publishing house,** ISBN: ISBN-13:978-3-659-66574-5, ISBN-10: 3659665746, EAN: 9783659665745.

[12] . Chen, B., & Soares, C. *Effect of welding sequence on temperature distribution, distortions, and residual stress on stiffened plates,* **The International Journal of Advanced Manufacturing Technology,** 2018, pp. 3145–-3156.

[13] Rajput, E., *Heat-and-mass-transfer.* (5th, Ed.) New Delhi: S. Chand & Company Ltd. 2012.